

A Determination Method of CO₂-Oil Miscible State in the Heterogeneous Low-Permeability Reservoir

Lili Jing^{1,2}, Leng Tian^{1,2*}, Can Huang^{1,2}, Jiaxin Wang^{1,2}, Zechuan Wang^{1,2}, Hengli Wang^{1,2}

1 State Key Laboratory of Petroleum Resources and Prospecting, China University of Petroleum (Beijing), Beijing 102249, China

2 Institute of Petroleum Engineering, China University of Petroleum (Beijing), Beijing 102249, China

ABSTRACT

CO₂ flooding can effectively enhance the recovery of low-permeability reservoirs and realize CO₂ storage. However, the strong heterogeneity of low permeability reservoirs makes it difficult to accurately determine the miscible state of CO₂ and oil. In this study, first, a PR-EOS is modified by considering the shifts of critical properties. Second, the parachor model is coupled with the modified PR-EOS to predict the minimum miscible pressure (MMP). Third, considering the multiple contact process between CO₂ and oil, a MMP prediction model based on the microscopic heterogeneity is established. Afterwards, the model calculation results are compared with the prior experimental results of CO₂ flooding to verify its applicability and superiority. Finally, the model is applied to the actual low-permeability reservoir to determine the miscible state of CO₂ and oil.

Keywords: CO₂-oil miscible state, CO₂ flooding, microscopic heterogeneity, carbon capture and storage, low-permeability reservoir

1. INTRODUCTION

Carbon capture, utilization and storage (CCUS) is currently considered the most promising technology for greenhouse gas emission reduction[1, 2]. CO₂-EOR, also known as CO₂ flooding, is a technology that uses CO₂ to enhance recovery while trapping CO₂ in the reservoir for a long term, referred to as CO₂ sequestration process[3, 4]. Therefore, CO₂ flooding is an effective means to realize the geological storage of CO₂, and the most effective way to reduce greenhouse gas emissions under current economic conditions.

In the oil industry, most of the CO₂-EOR projects were implemented in miscible phase (CO₂ miscible flooding)[5-7]. During the process of CO₂ flooding, the miscibility state of CO₂-oil can be judged by the minimum miscibility pressure (MMP), which not only affects the displacement efficiency, but also affects the CO₂ storage efficiency[8]. The microscopic

heterogeneity of the reservoir is an important factor affecting the fluid seepage ability[9, 10]. However, the pore-throat size of low-permeability reservoirs is mainly micro-nano-scale and has strong micro heterogeneity, which leads to complicated CO₂ occurrence states and seepage rules in different pore-throat structures[11, 12]. Therefore, it is difficult to accurately predict the MMP that meets the conditions of low-permeability reservoirs.

In this study, the modified PR EOS is combined with the Parachor model, and considering the multiple contact process of CO₂ and crude oil, a prediction model of minimum miscible pressure for CO₂ flooding in low-permeability reservoirs is established. Then, the model calculation results were compared with the prior experimental results of CO₂ flooding to verify its applicability and superiority. Finally, the model is applied to the actual heterogeneous low permeability reservoir to judge the miscibility state of CO₂ and oil. The result showed that this method can not only calculate the MMP distribution of the heterogeneous reservoirs, but also determine the miscible state at different production stages of the CO₂ flooding process.

2. MODELING AND THEORY

2.1 Modified equation of state

First, the basic form of the PR equation of state is shown as follows[13]:

$$P = \frac{RT}{V-b} - \frac{a}{V^2 + 2Vb - b^2} \quad (1)$$

Where P is the system pressure; T is the thermodynamic temperature; R is the universal gas constant; V is the molar volume; a is gravitational parameter; b is the volume parameter. The parameters a and b can be calculated by van der Waals mixing rule:

$$a = \sum_i \sum_j x_i x_j (a_i a_j)^{0.5} (1 - k_{ij}) \quad b = \sum_i x_i b_i \quad (2)$$

In the above equation x_i and x_j are the molar fractions of component i and component j ; k_{ij} is the binary interaction coefficient of component i and

component j ; $k_{ij} = k_{ji}$ and $k_{ii} = k_{jj} = 0$; a_i and b_i are the energy and volume parameters of component i , respectively. The parameters a_i and b_i can be determined from:

$$a_i = \frac{0.45724R^2T_{ci}^2}{P_{ci}} \left[1 + m_i \left(1 - \sqrt{T_{ri}} \right) \right]^2 \quad (3)$$

$$b_i = 0.0778 \frac{RT_{ci}}{P_{ci}} \quad (4)$$

$$m_i = 0.379642 + 1.54226\omega_i - 0.26992\omega_i^2 \quad (5)$$

Where P_{ci} and T_{ci} are the critical pressure and temperature of component i , respectively; T_{ri} is the comparison temperature of component i ; ω_i is the acentric factor of component i .

Low-permeability heterogeneous reservoirs are mostly developed with micro-nano-scale pore throats, which generate high capillary pressure and lead to adsorption hysteresis effect. This adsorption hysteresis effect obviously affects the critical properties and phase behavior of fluids[14-16]. The critical shift parameter is measured using the corresponding correlation proposed by Zarragoicoechea et al.[17]:

$$\Delta P_c^* = \frac{P_c - P_{cp}}{P_{cp}} = 0.9409 \frac{\sigma_{LJ}}{r_p} - 0.2415 \left(\frac{\sigma_{LJ}}{r_p} \right)^2 \quad (6)$$

$$\Delta T_c^* = \frac{T_c - T_{cp}}{T_{cp}} = 0.9409 \frac{\sigma_{LJ}}{r_p} - 0.2415 \left(\frac{\sigma_{LJ}}{r_p} \right)^2 \quad (7)$$

$$\sigma_{LJ} = 0.2443 \sqrt[3]{\frac{T_c}{P_c}} \quad (8)$$

Where ΔP_c^* and ΔT_c^* are the relative critical pressure and temperature shift due to confinement, respectively T_{cp} is the critical temperature in nanopores; P_{cp} is the critical pressure in nanopores; r_p is the radius of the mainstream throat; σ_{LJ} is the Lennard-Jones size diameter.

To get the PR EOS applicable to the low-permeability heterogeneous reservoir, equations (6)-(8) are substituted into equation (1), which relates the critical properties of the fluid to the formation parameters (r_p). When the oil-gas system is in phase equilibrium, according to the Rachford-Rice equation:

$$\sum_{i=1}^N (y_i - x_i) = \sum_{i=1}^N \frac{z_i(K_i - 1)}{1 + (K_i - 1)V} = 0 \quad (9)$$

The initial K-value of each component can be estimated from Wilson's equation[18]:

$$K_i = \frac{P_{ci}}{P} \exp \left[5.373(1 + \omega_i) \left(1 - \frac{T_{ci}}{T} \right) \right] \quad (10)$$

Where y_i and x_i are the molar fractions of component i in the vapour phase and liquid phase, respectively; K_i is the vapour-liquid equilibrium constant of component i ; V is the molar fraction of the vapour phase.

The fugacity coefficient of each component in the mixture is:

$$\varphi_i^v = \exp \left\{ \frac{b_i}{b} (Z_v - 1) - \ln \frac{P(V_v - b)}{RT} - \frac{a}{2.828RT} \times \left[\frac{2 \sum_{j=1}^n y_j (a_i a_j)^{0.5} (1 - k_{ij})}{a} - \frac{b_i}{b} \right] \ln \left(\frac{V_v + 2.414b}{V_v - 0.414b} \right) \right\} \quad (11)$$

$$\varphi_i^l = \exp \left\{ \frac{b_i}{b} (Z_L - 1) - \ln \frac{P(V_L - b)}{RT} - \frac{a}{2.828RT} \times \left[\frac{2 \sum_{j=1}^n x_j (a_i a_j)^{0.5} (1 - k_{ij})}{a} - \frac{b_i}{b} \right] \ln \left(\frac{V_L + 2.414b}{V_L - 0.414b} \right) \right\} \quad (12)$$

2.2 Parachor model

The liquid and vapour phases are set as the wetting and non-wetting phases, respectively, in the low-permeability reservoir[19]. The calculation formula of capillary pressure is as follows:

$$P_c = P_v - P_L = \frac{2\gamma \cos \theta}{r_p} \quad (13)$$

Where P_c is the capillary pressure; P_v and P_L are the pressure of vapour phase and liquid phase, respectively; γ is the interfacial tension; θ is the contact angle of the vapour-liquid interface.

During CO₂ flooding, the MMP is reached when the IFT between CO₂ and oil reduces to zero. The parachor model is most commonly used by the petroleum industry to predict the IFT of a liquid-vapour (e.g., oil-CO₂) system[20]:

$$\gamma = \left[\sum_{i=1}^n (\rho_L [p]_i x_i - \rho_v [p]_i y_i) \right]^4 \quad (14)$$

$$[p]_i = 176.05005 - 7472.9807V_c - 0.87458088T_c + 1560.4793H + 19.309439H^2 + 0.05013801H^3 - \frac{25.691718}{H} \quad (15)$$

$$H = V_c^{5/6} T_c^{0.25} \quad (16)$$

Where $[p]_i$ is the parachor of component i ; ρ_v and ρ_L are the molar densities of the bulk vapour and liquid phases, respectively; V_c is the critical molar volume; H is a function of T_c and V_c .

2.3 Multiple contact process

Based on the Kozeny-Calman equation, parameters such as porosity, tortuosity, and specific surface area of pores are quantitatively characterized by permeability[21]:

$$K = \frac{\phi^3}{2\tau^2 S^2} \quad (17)$$

The relationship between mainstream kindness and permeability is[22]:

$$K = 0.416r_p^{2.6481} \quad (18)$$

According to formula (8), the parameter of permeability is used to quantitatively characterize the heterogeneity of pore structure of low-permeability reservoirs.



Fig. 1 Schematic diagram of the unit and unit simulation

Crude oil and CO₂ must undergo multi-stage contact and mass transfer to achieve miscibility[23]. The diffusion effect between units and units is considered to determine the concentration of CO₂ along the seepage

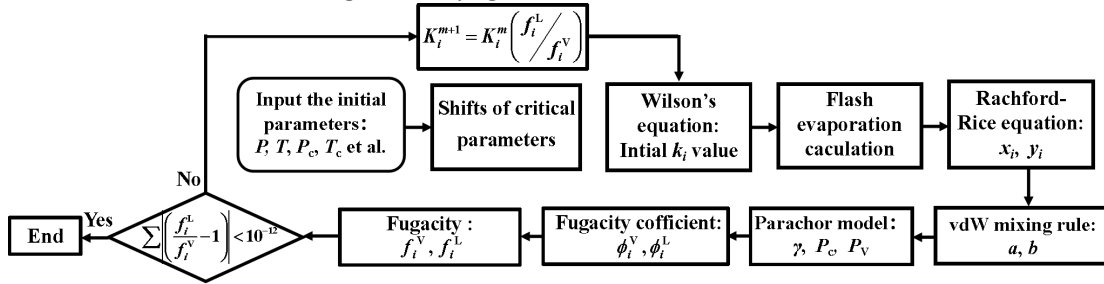


Fig. 2 Flowchart of the calculation process of minimum miscible pressure

3. RESULTS AND DISCUSSION

3.1 Model validation

Based on the model established above, the minimum miscible pressure of different throat radius measured by Rashid S.M et al was predicted[24]. The comparison between the predicted value of the model and Rashid S.M is shown in Table 1.

The error between the minimum miscible pressure predicted by the model and the previous experimental measurement results is 0.77% in the 5 nm throat and 0.93% in the 10 nm throat. This demonstrates that the MMP prediction model developed in this study is extremely accurate.

Table 1 Model Validation Results

| Throat radius | 5nm | | 10nm | |
|---------------|-----------------------|----------------------|-----------------------|------------------|
| | Results of Rashid S.M | MMP prediction model | Results of Rashid S.M | Prediction model |
| MMP | 19.37MPa | 19.52MPa | 21.40MPa | 21.60MPa |

3.2 Comparison of different minimum miscible pressure Determination Methods

in each unit and to obtain the mixing ratio of CO₂ and crude oil.

$$\frac{\partial c}{\partial t} + \varepsilon_x \frac{\partial c}{\partial x} + \varepsilon_y \frac{\partial c}{\partial y} = D_x \frac{\partial^2 c}{\partial x^2} + D_y \frac{\partial^2 c}{\partial y^2} \quad (19)$$

Where c is the concentration of the vapour phase in the liquid phase; dx , dy and dz are the length, width and height of a unit in Fig. 1; D is the diffusion coefficient of the vapour phase in the liquid phase; ε is the convection velocity.

The initial condition is:

$$c(x, y, 0) = 0 \quad x > x_0, y > y_0 \quad (20)$$

And the boundary condition is:

$$c(0, 0, t) = c_0, c(\pm\infty, \pm\infty, t) = 0 \quad 0 < t < \infty \quad (21)$$

The MMP needs to be calculated by a series of iterative computations, such as the Newton-Raphson method. Fig. 2 presents the flowchart of the calculation process.

Thin tube test, IFT test, numerical simulation, and MMP prediction model results are compared in this study. The oil samples in the experiment are all from the H3 reservoir in the Ordos Basin. The crude oil composition of the H3 reservoir is shown in Table 2.

Table 2 The crude oil composition of H3 oilfield

| | | | | | |
|-----------|-----------------|-----------------|-----------------|-----------------|----------------|
| Component | N ₂ | CO ₂ | C ₁ | C ₂ | C ₃ |
| Content,% | 0.77 | 0.08 | 26.72 | 8.16 | 8.53 |
| Component | iC ₄ | nC ₄ | iC ₅ | nC ₅ | C ₆ |
| Content,% | 1.42 | 5.23 | 1.92 | 2.69 | 3.32 |
| Component | C ₇ | C ₈ | C ₉₊ | - | - |
| Content,% | 3.74 | 4.95 | 32.47 | - | - |

The MMP measured by different methods is shown in Table 3. Firstly, the above four methods are divided into two categories. One is not considering the heterogeneity, such as IFT test, and the MMP is 21.63MPa (Fig. 3), which is the maximum value among these four methods. One is considering the heterogeneity, such as thin tube test, numerical simulation and MMP prediction model. Thin tube method has the largest permeability and the largest throat radius, which is relatively different from the actual reservoir, and the experimental results are shown in Fig. 4. In contrast, the MMP obtained by the

numerical simulation and the MMP prediction model is close because the pore size of the reservoir is similar. However, after determining the approximate range of MMP, the numerical simulation method needs to set different injection pressure for simulation. The MMP prediction model can be directly calculated by iteration, which is simple and easy to operate.

Table 3 MMP determined by different methods

| Method | Thin tube test | IFT test | Numerical simulation | Prediction model |
|--------|----------------|----------|----------------------|------------------|
| MMP | 20.3MPa | 21.4MPa | 18.0MPa | 18.35MPa |

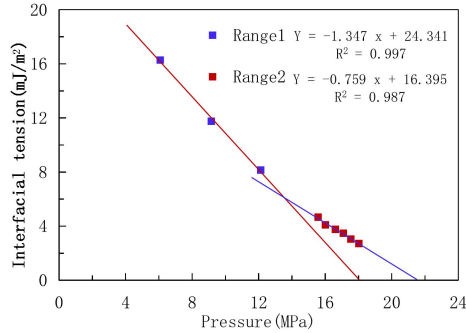


Fig. 3 Relationship between interfacial tension and equilibrium pressure in CO₂-crude oil system

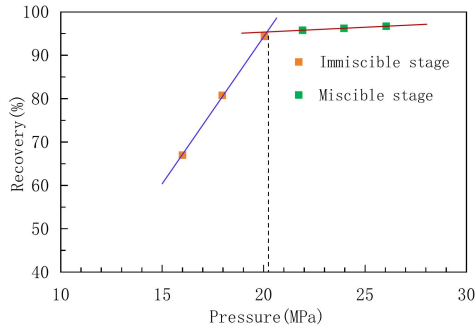


Fig. 4 Processing diagram of thin tube experimental results

3.3 Judgment of miscible state of the heterogeneous reservoir

The H3 reservoir is a typical low-porosity-ultra-low-porosity, low permeability reservoir. The Y30 well group, a typical well group in the H3 reservoir, was selected to analyze the distribution of MMP in the heterogeneous low-permeability reservoir and the location of CO₂ and crude oil miscible front and immiscible area during different production stages. The permeability in the well control area of the Y30 well group was reduced from 2.2 mD to 0.1 mD with a significant permeability heterogeneity (Table 4).

Table 4 Basic information of well group Y29-101

| Well ID | Type | Porosity | Permeability | Oil saturation |
|---------|----------|----------|--------------|----------------|
| Y30-2 | Injector | 7.76% | 0.56mD | 52.6% |

| | | | | |
|-------|----------|-------|--------|-------|
| Y30-9 | Producer | 8.11% | 0.83mD | 54.8% |
| Y30-8 | Producer | 7.93% | 0.23mD | 53.2% |
| Y30-7 | Producer | 7.88% | 0.15mD | 55.9% |
| Y30-3 | Producer | 8.01% | 1.56mD | 54.4% |
| Y30-1 | Producer | 7.69% | 0.13mD | 54.2% |
| Y30-6 | Producer | 8.21% | 1.72mD | 53.5% |
| Y30-5 | Producer | 8.25% | 0.68mD | 56.1% |
| Y30-4 | Producer | 7.88% | 0.16mD | 55.8% |

Firstly, the radius of the mainstream throat of each well in the Y30 well group was calculated based on the permeability. Then, the MMP of each well was calculated using the MMP prediction model, and the MMP distribution map was drawn based on the Kriging method (Fig. 5). The maximum MMP of this well group is located in the west area (MMP > 22.1 MPa), while the MMP in the east area of the well group is smaller (MMP < 19.8 MPa). During the slim tube experiment, the pressure when the final recovery rate reaches 90% is defined as the minimum miscible pressure. Similarly, it is defined that the formation pressure of more than 90% of the well control area of this well group exceed MMP is the best MMP corresponding to the whole well group, the MMP of the Y30 well group is 20.1 MPa.

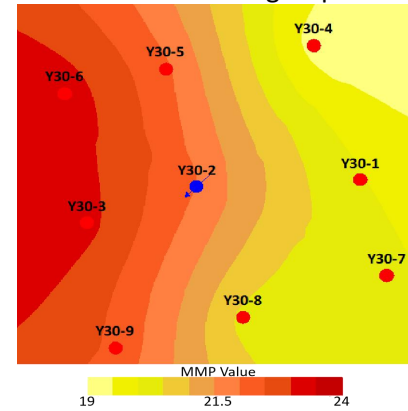


Fig. 5 The MMP distribution of Y30 well group

3.3.1 Unsteady flow stage

The miscible state of CO₂ and crude oil in different flow stages was determined using well Y30-2 and its adjacent well Y30-1 as examples. The two wells are 500 m apart. Selecting a certain time at the beginning of production, the formation pressure curve of well Y30-2 along the direction of well Y30-1 can be obtained from the monitoring data. The MMP prediction model can calculate the MMP at different positions between the two wells. Using Y30-2 as the origin and the well distance as the x-axis, the formation pressure curve and the MMP curve are plotted in the same coordinate system, e.g., Fig. 6.

Comparing the formation pressure curve with the MMP curve, the intersection point appears at the location 426 m from the injection well, indicating that

the front of the miscible phase is at the position roughly 426 m from the injection well (Fig. 6). The MMP in the area located beyond 426 is significantly higher than the formation pressure and cannot reach the miscible phase. At this time, the phase distribution between the two wells is shown in Fig. 7. Within 426 m from the injection well, there may be a CO₂-enriched area, as well as a miscible area. Beyond 426 m from the injection well, a immiscible area and a crude oil area may exist.

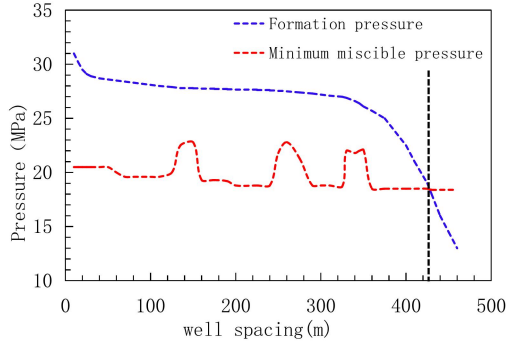


Fig. 6 Formation pressure vs. MMP in unsteady flow stage

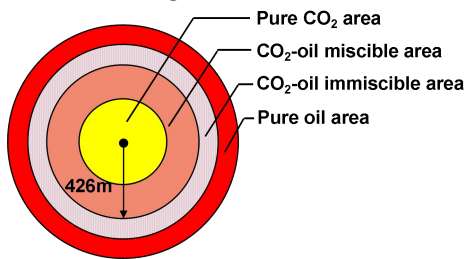


Fig. 7 Phase distribution in unsteady flow stage

3.3.2 Steady flow stage

In steady flow stage, the miscible front is 318 m away from the injection well, and most areas in the formation have reached the miscible state with the minimum miscible pressure of 19.8 MPa (Fig. 8).

During the steady flow stage, the phase state in the formation can be divided into three areas: the pure CO₂ area, the CO₂-oil miscible area, and the near-miscible-phase area (Fig. 9). However, at a distance of 200-300 m from the injection well, the MMP curve becomes convex, and the formation pressure has not yet reached the MMP. This is mainly due to the large permeability at this location, which leads to a large MMP, which also indicates that there is a local immiscibility phenomenon in the heterogeneous reservoir. Therefore, a local immiscible area is added in Fig. 9, which should also be the remaining oil enrichment area. In addition, the MMP at the miscible front is larger at this time, and the formation pressure in the area beyond 310 m from the injection well is close to the MMP, which may reach a near-miscible state.

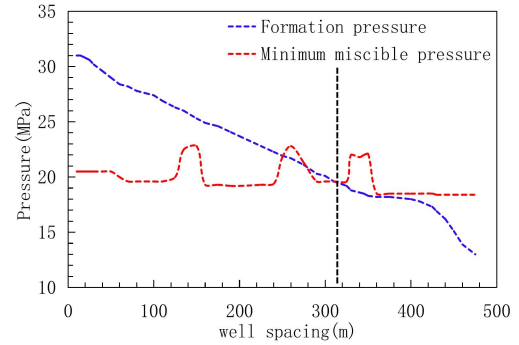


Fig. 8 Formation pressure vs. MMP in steady flow stage

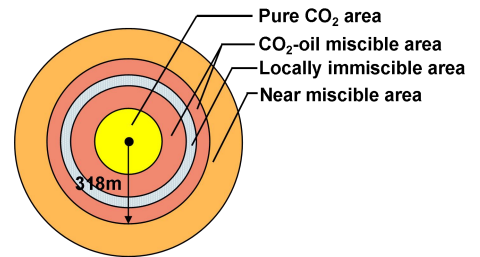


Fig. 9 Phase distribution in steady flow stage

4. CONCLUSIONS

1) The model calculation results are compared with the prior experimental results of CO₂ flooding to verify its applicability and superiority. The results showed that the difference between the MMP prediction model and the prior experimental results is 0.77% and 0.93%, respectively, indicating that the model was highly accurate.

2) The minimum miscible pressure of crude oil in H3 reservoir is determined by thin tube test, IFT test, numerical simulation method and MMP prediction model. The results show that the minimum miscible pressures obtained by different methods are quite different, and the minimum miscible pressures measured by the methods considering reservoir parameters are all smaller.

3) Comparing the formation pressure curves between injection and production wells in different stages with the MMP curves calculated by the model, it is judged that the front of miscible phase in the unstable flow stage is at 426 m from the injection well, and pure CO₂ area, CO₂-oil miscible area, immiscible area and pure oil area exist in the formation. In the steady flow stage, the miscible front is at 318 m from the injection well, and there are pure CO₂ area, CO₂-oil miscible area, locally immiscible area and near-miscible area in the formation.

4) Through the above study, it can be found that the size of the miscible area will primarily affect the final recovery rate. During the CO₂ displacement process, the MMP can be calculated by the MMP prediction model first, and then different injection pressure is set (injection pressure greater than MMP) to observe the propagation range of the pressure wave

and the range of the miscible-phase area during the steady flow stage, so as to determine the best injection pressure.

ACKNOWLEDGEMENT

The authors would like to thank the National Natural Science Foundation of China (Grant No.: 51974329) for the financial supports.

REFERENCE

- [1] Rezk MG, Foroozesh J, Zivar D, Mumtaz M. CO₂ storage potential during CO₂ enhanced oil recovery in sandstone reservoirs. *Journal of Natural Gas Science and Engineering* 2019;66:233-43.
- [2] Zheng YW, Gao L, Li S, Wang D. A comprehensive evaluation model for full-chain CCUS performance based on the analytic hierarchy process method. *Energy* 2022;239.
- [3] Shelton JL, McIntosh JC, Hunt AG, Beebe TL, Parker AD, Warwick PD, et al. Determining CO₂ storage potential during miscible CO₂ enhanced oil recovery: Noble gas and stable isotope tracers. *International Journal of Greenhouse Gas Control* 2016;51:239-53.
- [4] Wang HL, Tian L, Zhang KQ, Liu ZK, Huang C, Jiang LL, et al. How Is Ultrasonic-Assisted CO₂ EOR to Unlock Oils from Unconventional Reservoirs? *Sustainability* 2021;13(18).
- [5] Yu HY, Lu X, Fu WR, Wang YQ, Xu H, Xie QC, et al. Determination of minimum near miscible pressure region during CO₂ and associated gas injection for tight oil reservoir in Ordos Basin, China. *Fuel* 2020;263.
- [6] Choubineh A, Helalizadeh A, Wood DA. The impacts of gas impurities on the minimum miscibility pressure of injected CO₂-rich gas-crude oil systems and enhanced oil recovery potential. *Petroleum Science* 2019;16(1):117-26.
- [7] Xu B. CO₂ miscible flooding in low permeability sandstone reservoirs and its influence on crude oil properties. *Petroleum Science and Technology* 2017;35(21):2024-9.
- [8] Zhang KQ, Jia N, Li SY, Liu LR. Rapid Determination of Interfacial Tensions in Nanopores: Experimental Nanofluidics and Theoretical Models. *Langmuir* 2019;35(27):8943-9.
- [9] Wang HL, Tian L, Chai XL, Wang JX, Zhang KQ. Effect of pore structure on recovery of CO₂ miscible flooding efficiency in low permeability reservoirs. *Journal of Petroleum Science and Engineering* 2022;208.
- [10] Yin DY, Wang DQ, Zhou YZ, Zhang CL. Pore Structure Characteristics of Ultra-Low Permeability Reservoirs. *Natural Resources Research* 2021;30(1):451-62.
- [11] Wang Q, Yang SL, Glover PWJ, Lorinczi P, Qian K, Wang L. Effect of Pore-Throat Microstructures on Formation Damage during Miscible CO₂ Flooding of Tight Sandstone Reservoirs. *Energy & Fuels* 2020;34(4):4338-52.
- [12] Liu Y, Chen X. Miscible conditions of CO₂ flooding technology used in low permeability reservoirs. *Petroleum Exploration and Development* 2010;37(4):466-70.
- [13] Turkevich LA, Mann JA. Pressure dependence of the interfacial tension between fluid phases. 1. Formalism and application to simple fluids. *Langmuir* 1990;6(2):445-56.
- [14] Wu HH, Thibault CG, Wang H, Cychosz KA, Thommes M, Li J. Effect of temperature on hydrogen and carbon dioxide adsorption hysteresis in an ultramicroporous MOF. *Microporous and Mesoporous Materials* 2016;219:186-9.
- [15] Aharoni C. Interaction between adsorption and condensation processes in a pore and its effect on hysteresis. *Chemical Engineering Communications* 2002;189(4):429-35.
- [16] Diao R, Fan CY, Do DD, Nicholson D. On the adsorbate restructuring induced hysteresis of simple gas adsorption in slit micropores. *Chemical Engineering Journal* 2016;290:381-90.
- [17] Zarragoicoechea GJ, Kuz VA. Critical shift of a confined fluid in a nanopore. *Fluid Phase Equilibria* 2004;220(1):7-9.
- [18] Wilson GM. Vapor-liquid equilibrium. XI. A new expression for the excess free energy of mixing. *Journal of the American Chemical Society* 1964;86(2):127-30.
- [19] Nojabaei B, Johns RT, Chu L. Effect of Capillary Pressure on Phase Behavior in Tight Rocks and Shales. *Spe Reservoir Evaluation & Engineering* 2013;16(3):281-9.
- [20] Nobakht M, Moghadam S, Gu YG. Determination of CO₂ Minimum Miscibility Pressure from Measured and Predicted Equilibrium Interfacial Tensions. *Industrial & Engineering Chemistry Research* 2008;47(22):8918-25.
- [21] Lu H, Guo J, Wang Y, Yang M, Nan W. Trapping Damage Analysis of Water Locking/Aqueous Phase of Tight Sandstone Gas Reservoir in Ke Keya Structure. *IADC/SPE Asia Pacific Drilling Technology Conference and Exhibition*. OnePetro; 2012.
- [22] Meng H, Liu TY. Interpretation of the rock-electric and seepage characteristics using the pore network model. *Journal of Petroleum Science and Engineering* 2019;180:1-10.
- [23] Chen H, Liu XL, Zhang C, Tan XH, Yang R, Yang SL, et al. Effects of miscible degree and pore scale on seepage characteristics of unconventional reservoirs fluids due to supercritical CO₂ injection. *Energy* 2022;239.
- [24] Mohammad RS, Zhang SC, Ehsan ul H, AlQadasi AM. Investigation of Cyclic CO₂ Injection Process with Nanopore Confinement and Complex Fracturing Geometry in Tight Oil Reservoirs. *Arabian Journal for Science and Engineering* 2018;43(11):6567-77.